Microstructure transformation and mechanical properties of Al alloy joints soldered with Ni-Cu foam/Sn-3.0Ag-0.5Cu (SAC305) composite solder

Cong Xiong [a], Yong Xiao [a*], Jian Zhang [b], Dan Luo [c*], Russell Goodall [c]

a. School of Materials Science and Engineering, Wuhan University of Technology, Wuhan, 430070, China

b. State Key Laboratory of Advanced Technology for Materials Synthesis and Processing, Wuhan University of Technology, Wuhan 430070, China

c. Department of Materials Science and Engineering, The University of Sheffield, Sheffield, S1 3JD, UK

*Corresponding author, E-mail address: yongxiao@whut.edu.cn

*Corresponding author, E-mail: d.luo@sheffield.ac.uk

Abstract

In this study, Ni-Cu/SAC composite solders with different Cu contents were used as an interlayer to solder Al alloy joints at 250 °C for different time. The results showed that the formation and evolution of the microstructure were affected by the Cu contents. In the Ni18Cu/SAC joint, the Sn solder was completely consumed to form a solid-phase joint in 5 min. And $(Cu,Ni)_6Sn_5$ was the initial phase formed from the reaction between Sn solder and the Ni18Cu skeleton. Due to the higher Ni concentration than $(Cu,Ni)_6Sn_5$ phase in the Ni18Cu skeleton, the Ni atoms diffused from Ni18Cu skeleton to the $(Cu,Ni)_6Sn_5$ phase and replaced the Cu atoms in it. As a result, the content of Ni atoms in $(Cu,Ni)_6Sn_5$ phase increased continuously, and transformed into $(Ni,Cu)_3Sn_4$ at 10 min. Phase transition also occurred in the Ni38Cu/SAC joints. However, the initial phase formed from the reaction between Sn solder and the Ni38Cu skeleton was

(Ni,Cu)$_3$Sn$_4$. Therefore, the (Ni,Cu)$_3$Sn$_4$ phase was transformed into (Cu,Ni)$_6$Sn$_5$ at 10 min because the Cu atoms diffused from Ni38Cu skeleton to (Ni,Cu)$_3$Sn$_4$. On increasing the soldering time, the shear strength of the joints first increased and then decreased, the Ni18Cu/SAC joints soldered for 10 min exhibited the highest shear strength of 58.3 MPa, the shearing failure mainly happened in the composite solder layers.

Keywords: Foam reinforced solders; Ni-Cu/SAC composite solder; Al joint; Solid-phase transitions; Microstructure; Mechanical properties

1 Introduction

Al alloys, exhibiting high strength, low density, and good electrical conductivity, are commonly used in radio-frequency and microwave high-frequency devices. At present, some metal layers are electroplated on the Al alloys surface to improve the wettability of high-frequency devices, then soldered with Sn-based solder at low temperatures. However, the development of functional integration and volume miniaturization of high-frequency devices puts forward higher requirements for the soldered joints [1-3]. For example, some complex multilayer devices facing gradient welding require excellent thermal stability [4-6], which can be solved by transient liquid phase (TLP) soldering.

In recent years, TLP soldering was considered to be a promising way to fabricate high melting points joints because of the process characteristics of "low-temperature welding and high-temperature service" [7-9]. TLP is usually a sandwich structure assembled with a low melting point solder interlayer and two high melting point

2

substrates, such as Ni/Sn/Ni [10], Ag/Sn/Ag [11], Cu/Sn/Cu [12], and Cu/Sn/Ni [13]. The intermetallic compounds (IMCs) with high melting points are formed by the metallurgical reactions between substrates and the Sn solder to realize the connection of brazing joints. Nevertheless, the traditional TLP usually takes tens of minutes or even longer to completely consume the solder and form the full-IMC [3, 10], resulting in the base materials being excessively corroded and the production of thermal stress. It is more serious for high-frequency devices with thin electroplated metal layers. Furthermore, Cheng [14] found some cavities were appeared in the joints caused by the volume shrinkage while the Sn solder was exhausted and full-IMC was formed. The cavities induced by volume shrinkage and the thermal stress induced by the long reaction time could decrease the strength of the joints [10, 15]. To shorten the soldering time and remove the cavities, Shao [16] used a solder sheet pressed by mixing Cu and Sn powder to solder the Cu joints. As a result, a high melting point joint comprising of Cu_6Sn_5, Cu_3Sn, and Cu particles was obtained, but the maximum shear strength of the joints was only 32.9 MPa. It is difficult to obtain a high strength joint by using the traditional Sn-based solder. Therefore, it is necessary to develop a new type of solder to shorten the soldering time and obtain a joint with excellent mechanical properties.

Metal foam, exhibiting high strength, good toughness and large surface area, is widely used in electrocatalysis [17], alloy strengthening [18], sound insulation [19] and energy absorption [20]. For example, Zhang [21] fabricated the Cu-foam reinforced Sn-Bi solder and found the Cu foam not only refined the solder structure but also enhanced the mechanical properties of the Sn-Bi solder. The Ni foam-Sn/Cu joints were

fabricated in our previous work [22-24]. The Sn solder was quickly consumed by the metallurgical reactions between Sn solder and Ni foam, forming a high melting point joint containing $(Ni,Cu)_3Sn_4$, $(Cu,Ni)_6Sn_5$ and Ni skeleton. The mechanical properties of joints were significantly improved by the double interpenetrating structure effects of the ductile Ni skeleton and the brittle IMCs [25]. On increasing the time, the $(Cu,Ni)_6Sn_5$ was transformed into $(Ni,Cu)_3Sn_4$ and the grains were simultaneously refined, ultimately enhancing the mechanical properties of the joints. However, the phase transition mechanism of the metallurgical reaction phases in the above mentioned joints is not clear in existing studies. In addition, the existing research is mainly based on the development of pure Ni foams, which can take a long time to form a high melting point joint due to the low reaction rate of the Ni/Sn solid-liquid interface. Numerous studies showed that Cu doping in the Ni-Cu alloys could accelerate the metallurgical reaction rate and improve the reactions with Sn matrix [26-29]. Therefore, it is expected to control the metallurgical reaction behaviors by selecting the Ni-Cu alloy foam and adjusting its composition.

In this work, Ni-Cu/SAC305 composite solders with different Cu contents were used as an interlayer to solder Al alloy joints at 250 °C for different time. The microstructure evolution and mechanical properties of the joints were studied. The mechanisms of microstructure evolution and mechanical property strengthening were discussed. This work provides a new idea for obtaining a high strength Al alloy joint soldered at low temperatures.

2 Experimental materials and methods

Al substrate with a dimension of φ5 mm×3 mm was electroplated with Ni, Cu, Ag layers with a thickness of 9 μm, 2 μm, and 7 μm, respectively. The Cu layer was electroplated on the surface of the Ni foam (the thickness, porosity, and purity were 0.5 mm, 60 %, and 99.9 wt.%, respectively) by ultrasonic electroplating with a plating current density of 6 A/dm^2. The Cu content was controlled by the plating time, and the Cu content was 18 wt.% and 38 wt.% at 30 min and 90 min, respectively. Then the Ni-Cu alloy foam was prepared by sintering at 900 °C for 4 h in a vacuum environment. Subsequently, the Ni-Cu alloy foam was filled with Sn-3.0Ag-0.5Cu (wt.%, SAC305) solder after being immersed in a molten SAC305 solder at 240 °C for 2 min. Finally, the composite solder was rolled to foils with a thickness of 80 μm by an electric rolling machine (Kejing Co., Ltd., MSK-2150).

Prior to the soldering process, composite solder foils and Al substrates were ultrasonically cleaned in absolute ethanol to remove the impurities on the surface. After applying the flux, composite solder foils and Al substrates were assembled as a sandwich structure shown in **Fig. 1**a. The samples were soldered at 250 °C for 1 min, 5 min, 10 min, and 15 min in a vacuum furnace, respectively. Then the as-soldered joints were taken out at 200 °C and cooled to room temperature in air.

The as-soldered joints and shear-failed joints were installed in epoxy resin, and then the cross-sections were observed after grinding and polishing. The microstructure and elemental compositions of the joints were characterized by an electron-probe micro-analyzer (EPMA, JEOL JXA-8230) equipped with an energy dispersive X-ray spectrometer (EDS, INCAX-ACT). To further observe the microstructure evolution of

the joints, electron backscatter diffraction (SEM/EBSD, JEOL JSM-7001F) was used to characterize the phase and the grain distribution. The shear strength of the joints was tested by an electronic universal testing machine (MTS-E44.104) with a tensile speed of 0.5 mm/min at room temperature. The schematic diagram for the shearing test sample and fixture is shown in **Fig. 1**b. Five samples were tested for each experimental parameter to obtain an average strength value.

3 Results and Discussion

3.1 Microstructure of composite solder

Fig. 2 shows the cross section images of the Ni-Cu skeleton and Ni-Cu/SAC composite solders. As shown in **Fig. 2**a and **Fig. 2**b, the Cu layer was attached to the surface of the Ni foam and bonded well with it. **Fig. 2**c and **Fig. 2**d show the EPMA images of Ni18Cu/SAC and Ni38Cu/SAC composite solders. It can be found that the Ni-Cu alloy foam still maintains a three-dimensional continuous network structure and distributed in the SAC305 solder matrix. The Ni-Cu alloy foam is well combined with the solder matrix without voids and cracks. Due to more pores in the Ni18Cu skeleton, the Ni18Cu/SAC composite solder contains more Sn solder than Ni38Cu/SAC composite solder.

3.2 Formation of IMCs in solid-liquid interfacial reaction stage

Fig. 3 shows the SEM images of cross-section microstructure and EBSD images for phase and grain distribution of Ni18Cu/SAC and Ni38Cu/SAC joints for 1 min. Strong metallurgical reactions occur inside the composite solder and at the solder/Al substrate interface. According to the EDS analysis results shown in **Table 1**, the IMCs

inside the composite solders, e.g. $(Cu,Ni)_6Sn_5$ (A1) and $(Ni,Cu)_3Sn_4$ (A2), are formed by the reaction between the Sn solder and Ni-Cu skeleton.

As shown in **Fig. 3**a, the Ni18Cu/SAC joint was composed of Ag_3Sn, $(Cu,Ni)_6Sn_5$, Ni18Cu skeleton, and Sn solder. Continuous Ag_3Sn layers are formed at the Ag layer/Sn solder interface. The $(Cu,Ni)_6Sn_5$ phase is mainly attached to the Ni18Cu skeleton surface and part of $(Cu,Ni)_6Sn_5$ disperses in the solder. As to the Ni38Cu/SAC joint (**Fig. 3**b), the IMC formed between the Sn solder and Ni38Cu skeleton was identified as $(Ni,Cu)_3Sn_4$, which attaches to the Ni38Cu skeleton. It can be seen from **Fig. 3**a_3 and **Fig. 3**b_3 that the Sn grains in Ni38Cu/SAC joint are much larger than those of Ni18Cu/SAC joint. The average grain size was calculated by Aztec Crystal software (Oxford instrument). The average sizes of Sn grains in Ni18Cu/SAC joint and Ni38Cu/SAC joint are 1.42 μm and 2.75 μm, respectively. The finer Sn grains in the Ni18Cu/SAC joint are attributed to the distribution of $(Cu,Ni)_6Sn_5$ in the solder, which inhibits the coarsening of Sn grains.

The formation and distribution of $(Cu,Ni)_6Sn_5$ in the Ni18Cu/SAC joint for 1 min can be related to the concentration change of Cu atoms in the Sn solder. It was reported that the diffusion rate of Cu atoms in Sn solders ($2.5×10^{-7}$ cm^2/s) was two orders of magnitude higher than that of Ni atoms ($5.4×10^{-9}$ cm^2/s) [30-32]. In addition, the solubility of Cu atoms in Sn solder was 1.2 wt.%, which was also higher than that of Ni atoms (less than 0.2 wt.%) [30]. Consequently, the Cu atoms has a higher diffusion rate from Ni18Cu skeleton to molten Sn solder than Ni atoms, inducing that the Cu atoms concentration in Sn solder is much higher than that of Ni atoms. Ho [33] studied

the effects of Cu atoms concentration on the reactions between Ni substrates and Sn-Ag-Cu solders. The results showed that only a continuous $(Cu,Ni)_6Sn_5$ layer was formed on the surface of Ni substrate when the Cu atoms concentration in Sn-Ag-Cu solder exceeded 0.6 wt.%. Therefore, the $(Cu,Ni)_6Sn_5$ is first formed in **Fig. 3**a_1 due to the higher Cu concentration in the Sn solder. However, the growth of $(Cu,Ni)_6Sn_5$ layer restricts the supply of Cu atoms from the Ni18Cu skeleton, resulting in severe consumption of the Cu atoms in the Sn solder during the formation of $(Cu,Ni)_6Sn_5$. Therefore, part of $(Cu,Ni)_6Sn_5$ phase detaches from the IMC layer and disperses in the Sn solder due to the decrease of the Cu concentration. The same results can be found in the previous literature reported by Wang[28].

The formation of $(Ni,Cu)_3Sn_4$ in the Ni38Cu/SAC joint soldered for 1 min can owe to large quantities of Ni atoms dissolves in the Sn solder. According to the phase diagram of Cu-Ni binary alloy, the melting point of Ni-Cu alloy decreases due to the increase of Cu content, which means that Ni38Cu skeleton has a faster dissolution rate than Ni18Cu skeleton, inducing that more Ni atoms dissolves in Sn solder matrix within the same time. According to the Sn-rich corner of the Cu-Ni-Sn phase diagram, the Ni atoms can reduce the concentration of Cu in Sn solder. The results obtained by Vuorinen et al. [34] showed that the $(Ni,Cu)_3Sn_4$ phase was more stable than $(Cu,Ni)_6Sn_5$ when the Cu content was less than about 0.4 wt.% at 250 ℃. In addition, the dissolution of Ni slowed down the migration of Cu and Ni atoms in the solder, resulting in Cu and Ni atoms staying relatively close to the solid/liquid interface. Therefore, the $(Ni,Cu)_3Sn_4$ phase was attached to the Ni38Cu skeleton in the Ni38Cu/SAC joint soldered for 1 min.

The formation and growth of $(Ni,Cu)_3Sn_4$ can be divided into three stages. In the dissolution reaction stage, Cu and Ni atoms dissolves from the Ni38Cu skeleton into the Sn solder. Then, a small amount of $(Ni,Cu)_3Sn_4$ particles is formed on the surface of the Ni38Cu skeleton to reduce the nucleation energy, as shown in **Fig. 4**a. In the dissolution-diffusion stage, the non-continuous $(Ni,Cu)_3Sn_4$ is formed on the surface of the Ni38Cu skeleton. The growth of $(Ni,Cu)_3Sn_4$ is affected by the dissolution reaction and the diffusion rate of Ni, Cu, and Sn atoms through $(Ni,Cu)_3Sn_4$ grain boundary (GB), as shown in **Fig. 4**b. The reaction is the GB diffusion stage when $(Ni,Cu)_3Sn_4$ further grows to a continuous dense layer, as shown in **Fig. 4**c. Due to the barrier effects of $(Ni,Cu)_3Sn_4$ layer on the diffusion of Cu and Ni atoms[35, 36], the growth of $(Ni,Cu)_3Sn_4$ is dominated by GB diffusion of Sn atoms. Therefore, the growth rate of $(Ni,Cu)_3Sn_4$ gradually slows down.

In Ni18Cu/SAC joint, the detachment of $(Cu,Ni)_6Sn_5$ can reduce the distance between Sn solder and Ni18Cu skeleton to accelerate the reaction. But in Ni38Cu/SAC joint, the dense $(Ni,Cu)_3Sn_4$ layer not only hinders the diffusion rate of Ni and Cu atoms but also increases the diffusion distance, resulting in the decrease of reaction rate between Ni38Cu skeleton and Sn solder. Therefore, there is more residual Sn solder in the Ni38Cu/SAC joint than Ni18Cu/SAC joint in **Fig 3**.

3.3 Phase transition in solid-phase diffusion stage

Fig. 5 shows the cross-section images of Ni18Cu/SAC and Ni38Cu/SAC joints soldered for 5 min, 10 min, and 15 min, respectively. The Sn solder was completely consumed within 5 min, forming the joints composed of IMCs and Ni-Cu skeleton. It

can be seen from **Table 2**, the phase from the reaction between the Sn solder and Ni18Cu skeleton is dense $(Cu,Ni)_6Sn_5$ phase (B1) in 5 min. With prolonging soldering time to 10 min and 15 min, the reaction phase is $(Ni,Cu)_3Sn_4$ phase (B2 and B3). The $(Ni,Cu)_3Sn_4$ phase is loose due to the volume change caused by the phase transition. It is interesting that the phase from the reaction between Ni38Cu skeleton and Sn solder is $(Ni,Cu)_3Sn_4$ (B4) for 5 min and is $(Cu,Ni)_6Sn_5$ (B5 and B6) for both 10 min and 15 min.

Fig. 6 shows the phase and grain distribution of Ni18Cu/SAC joints soldered for 5 min, 10 min, and 15 min, respectively. As can be seen in **Fig. 6**a_1, $(Cu,Ni)_6Sn_5$ is the main phase from the reaction between the Sn solder and Ni18Cu skeleton is widely distributed in the seam when soldering for 5 min. A small amount of $(Ni,Cu)_3Sn_4$ particles is dispersed between the Ni18Cu skeleton and $(Cu,Ni)_6Sn_5$. With prolonging soldering time to 10 min and 15 min, the phase from the reaction between the Sn solder and Ni18Cu skeleton is only $(Ni,Cu)_3Sn_4$, as shown in **Fig. 6**a_2 and **Fig. 6**a_3.

As shown in **Fig. 3**a_2, the initial phase from the reaction between the Ni18Cu skeleton and the Sn solder is only $(Cu,Ni)_6Sn_5$. Therefore, it can be deduced that the $(Ni,Cu)_3Sn_4$ particles in **Fig. 7**a_1 are transformed from $(Cu,Ni)_6Sn_5$. As seen in **Table 2**, the Ni content of $(Cu,Ni)_6Sn_5$ in **Fig. 5**a_1 (B1) is 26.51 at.%, much lower than that of the Ni18Cu skeleton. Driven by the great Ni concentration gradient between Ni18Cu skeleton and $(Cu,Ni)_6Sn_5$, a mass of Ni atoms diffuses from Ni18Cu skeleton to the surface of $(Cu,Ni)_6Sn_5$ grains through grain boundary and bulk diffusion. Then the Ni atoms enter $(Cu,Ni)_6Sn_5$ grains and substitute for Cu atoms. The results of Yang et al.

[37] and Yoon et al. [38] showed that the $(Cu,Ni)_6Sn_5$ was transformed into $(Ni,Cu)_3Sn_4$ once the Ni concentration in $(Cu,Ni)_6Sn_5$ exceeded 24 at.%. In addition, the Cu content of $(Cu,Ni)_6Sn_5$ is 27.67 at.%, also higher than that of the Ni18Cu skeleton. Due to the Cu concentration gradient, the phase transition from $(Cu,Ni)_6Sn_5$ to $(Ni,Cu)_3Sn_4$ would be accelerated. Considering the diffusion distance, the $(Cu,Ni)_6Sn_5$ grains near Ni18Cu skeleton are first transformed into $(Ni,Cu)_3Sn_4$, as shown in **Fig 6a₁**.

With increasing soldering time to 10 min, the $(Cu,Ni)_6Sn_5$ is completely transformed into $(Ni,Cu)_3Sn_4$, as shown in **Fig. 6a₂**. It can be seen that the Ni content of $(Ni,Cu)_3Sn_4$ in **Fig. 5a₂** (B2) is 36.80 at.%, much lower than the one of Ni18Cu skeleton. Thus, Ni atoms can still diffuse from Ni18Cu skeleton to $(Ni,Cu)_3Sn_4$ due to the Ni concentration gradient. Subsequently, the Ni atoms gradually enter the $(Ni,Cu)_3Sn_4$ grains and substitute them for Cu atoms, resulting in a decrease of the Cu content in $(Ni,Cu)_3Sn_4$. The Cu content of $(Ni,Cu)_3Sn_4$ in the joint soldered for 15 min decreases from 6.58 at.% (B2) to 4.92 at.% (B3), which can contribute to the stability of $(Ni,Cu)_3Sn_4$. Therefore, with prolonging soldering time to 15 min, the reaction phase is still $(Ni,Cu)_3Sn_4$, as shown in **Fig. 6a₃**.

Fig. 7 shows the phase and grain distribution of Ni38Cu/SAC joints soldered for 5 min, 10 min and 15 min, respectively. It can be seen that the evolution of the reaction phase between the Sn solder and Ni38Cu skeleton is different from that in Ni18Cu/SAC joints. As seen in **Fig. 7a₁**, the joint is composed of $(Ni,Cu)_3Sn_4$, Ag_3Sn, and Ni38Cu skeleton after the Sn solder is completely consumed for 5 min. The reaction phase between the Sn solder and Ni38Cu skeleton is only $(Ni,Cu)_3Sn_4$ without $(Cu,Ni)_6Sn_5$.

11

On increasing the soldering time to 10 min, the reaction phase in the seam is only $(Cu,Ni)_6Sn_5$, as shown in **Fig. 7**a_2. It can be deduced that the $(Cu,Ni)_6Sn_5$ is transformed from $(Ni,Cu)_3Sn_4$. As seen in **Table 2**, the Cu content of $(Ni,Cu)_3Sn_4$ in **Fig. 5**b_1 (B4) is 11.73 at.%, much lower than that of Ni38Cu skeleton. Driven by the Cu atoms concentration gradient between Ni38Cu skeleton and $(Ni,Cu)_3Sn_4$, the Cu atoms massively diffuses from Ni38Cu skeleton to $(Ni,Cu)_3Sn_4$ surface through grain boundary and bulk diffusion. Then Cu atoms enter the $(Ni,Cu)_3Sn_4$ grains and substitute for Ni atoms. As a result, the $(Ni,Cu)_3Sn_4$ is transformed into $(Cu,Ni)_6Sn_5$ once the Cu concentration in $(Ni,Cu)_3Sn_4$ exceeded 8.5 at.%. It is consistent with the results of Yang et al. [30] and Ren et al. [39]. Due to the phase transition from $(Ni,Cu)_3Sn_4$ to $(Cu,Ni)_6Sn_5$, the concentration between the reaction phase and Ni38Cu skeleton is changed. As seen in **Table 2**, the Cu content of $(Cu,Ni)_6Sn_5$ in **Fig. 5**b_2 (B5) increases to 29.79 at.% and the Ni content decreases to 22.61 at.% in the joint soldered for 10 min. This means the diffusion rate of the Cu atoms from Ni38Cu skeleton to $(Cu,Ni)_6Sn_5$ would decrease due to the diminished Cu concentration gradient. While, the diffusion rate of the Ni atoms would increase correspondingly, resulting in an improved Ni content in $(Cu,Ni)_6Sn_5$ during longer soldering time. Therefore, the Ni content of $(Cu,Ni)_6Sn_5$ in the joint soldered for 15 min increases to 25.40 at.%, and the Cu content decreases to 28.44 at.%. And part of $(Cu,Ni)_6Sn_5$ grains is even transformed into $(Ni,Cu)_3Sn_4$, distributing between Ni38Cu skeleton and $(Cu,Ni)_6Sn_5$, as shown in **Fig. 7**a_3.

Fig. 8 shows the average size of $(Ni,Cu)_3Sn_4$ and $(Cu,Ni)_6Sn_5$ grains soldered at

various times. The average grain size was calculated by Aztec Crystal software (Oxford instrument). With increasing soldering time from 5 min to 10 min and then to 15 min, the average sizes of $(Cu,Ni)_6Sn_5$ and $(Ni,Cu)_3Sn_4$ grains in Ni18Cu/SAC and Ni38Cu/SAC joint both first decrease then increase. The joints soldered for 10 min exhibit the finest grain size of 1.52 μm and 1.49 μm, which decrease approximately by 10.06 % and 13.37 % comparing with the grains soldered for 5 min. The refinement of grains can be attributed to the phase transition. During the phase transition process, the previous rough phase decomposes and the new finer phase is formed. Due to the high nucleation rate of the new phase, the joints soldered for 10 min exhibits finer grains size. While further increasing the soldering time can result in the coarsening of the reaction phase and the increase of grains size.

3.3 Mechanical properties of solder joints

In order to evaluate the effects of microstructure on the mechanical properties of Al joints soldered with different Ni-Cu/SAC composite solders, shearing tests were conducted. **Fig. 9** shows the shear strength of Ni18Cu/SAC and Ni38Cu/SAC joints for various times. It can be seen that the shear strength first increases and then decreases in two kinds of joints. When soldering for 10 min, the Ni18Cu/SAC and Ni38Cu/SAC joints exhibit the highest shear strength of 58.3 MPa and 52.71 MPa respectively, increased approximately by 77 % and 51.7 % compared with the reported research [16].

Fig. 10 and **Fig. 11** show the cross-section and top-view SEM images of Al joints after shearing failure. It can be found that the shearing failure in Ni18Cu/SAC joints mainly occurred in the Ni-Cu skeleton and IMCs layer in **Fig. 10**a_1-a_4 and **Fig. 11**a_1-a_4.

This means that the shear strength of the Ni18Cu/SAC joint is closely related to the skeleton and IMCs. When soldering for 5 min, the double interpenetrating network structure comprised of the skeleton and IMCs can hinder and offset the cracks, which greatly improves the mechanical properties of the joints [25]. Increasing the soldering time to 10 min, the higher shear modulus of $(Ni,Cu)_3Sn_4$ would result in a further increase in the shear strength of the joints (the reported shear modulus of $(Ni,Cu)_3Sn_4$ and $(Cu,Ni)_6Sn_5$ are 4.48×10^{10} N/m^2 and 3.70×10^{10} N/m^2, respectively [40]). The area fraction of different phases in Ni-Cu/SAC joints soldered for various time were calculated by Aztec Crystal software (Oxford instrument), and the results are shown in **Table** 3. With the increase of soldering time, the area fractions of $(Ni,Cu)_3Sn_4$ and $(Cu,Ni)_6Sn_5$ in the joints remain unchanged, but the area of Ni-Cu alloy skeleton gradually decreases. The excessive consumption of Ni-Cu alloy foam would reduce the shear strength of the joints. Therefore, the shear strength of the joints soldered for 15 min decreases.

Fig. 10b1-b4 and **Fig. 11**b1-b4 show the cross-section and top-view SEM images of Ni38Cu/SAC joints. It can be found that the failure of the Ni38Cu/SAC joints soldered for 1 min and 5 min mainly occurred at the $(Ni,Cu)_3Sn_4/Ag_3Sn$ interface, as shown in **Fig. 10**b1-b2 and **Fig. 11**b1-b2. Residual stress would accumulate at the interface of $(Ni,Cu)_3Sn_4$ and Ag_3Sn because of the large mismatch of coefficient of thermal expansion (CTE) between them [41]. Moreover, the larger Sn grain size also reduces the shear strength of the joints. Therefore, the shear strength of Ni38Cu/SAC joints soldered for 1 min and 5 min is lower than that of Ni18Cu/SAC joints. When soldering

for 10 min, the $(Ni,Cu)_3Sn_4$ is transformed into $(Cu,Ni)_6Sn_5$, resulting in a reduced CTE mismatch at the interface. Therefore, the shear failures are shifted to the seam of the joints and the shear strength increases.

4 Conclusion

In this study, Al alloy joints were bonded with Ni18Cu/SAC and Ni38Cu/SAC composite solders at 250°C. The microstructure evolution and mechanical properties of the joints were investigated. The main results are as follows:

(1) In Ni18Cu/SAC joints, the initial intermetallic compounds (IMCs) from the reaction between the Sn solder and Ni18Cu skeleton was $(Cu,Ni)_6Sn_5$. On increasing the soldering time to 10 min and 15 min, the $(Cu,Ni)_6Sn_5$ was completely transformed into $(Ni,Cu)_3Sn_4$.

(2) In Ni38Cu/SAC joints, the initial IMCs from the reaction between the Sn solder and Ni38Cu skeleton was $(Ni,Cu)_3Sn_4$. And the $(Ni,Cu)_3Sn_4$ was completely transformed into $(Cu,Ni)_6Sn_5$ during soldering for 10 and 15 min.

(3) The difference in the formation of the initial IMC between two different joints is caused by the concentration of Ni and Cu atoms in the Sn solder. On increasing the soldering time, a phase transition occurs in both joints due to the diffusion of Cu and Ni atoms from the Ni-Cu skeleton to IMCs.

(4) The shear strength of Ni18Cu/SAC and Ni38Cu/SAC joints first increased and then decreased, the highest shear strength was 58.3 MPa and 52.71 MPa, respectively. It could be attributed to the refinement of the phase grains caused by the phase transition and the double interpenetrating strengthening effects of the ductile Ni-Cu skeleton and

the IMCs.

References

[1] R. Tian, C. Hang, Y. Tian, J. Feng, Brittle fracture induced by phase transformation of Ni-Cu-Sn intermetallic compounds in Sn-3Ag-0.5Cu/Ni solder joints under extreme temperature environment, Journal of Alloys and Compounds, 777 (2019) 463-471.

[2] H.W. Yang, J.Y. Wu, Z.X. Zhu, C.R. Kao, Effects of surface diffusion and reaction-induced volume shrinkage on morphological evolutions of micro joints, Materials Chemistry and Physics, 191 (2017) 13-19.

[3] H. Ji, M. Li, S. Ma, M. Li, Ni_3Sn_4-composed die bonded interface rapidly formed by ultrasonic-assisted soldering of Sn/Ni solder paste for high-temperature power device packaging, Materials & Design, 108 (2016) 590-596.

[4] P. Yao, P. Liu, J. Liu, Effects of multiple reflows on intermetallic morphology and shear strength of SnAgCu–xNi composite solder joints on electrolytic Ni/Au metallized substrate, Journal of Alloys and Compounds, 462 (2008) 73-79.

[5] B. Chen, Y. Huang, S. Tang, W. Liu, Y. Ma, Effects of multiple reflows on microstructure and shear strength of (Au-20Sn)-2Ag/Au/Ni(P)/Kovar joints, Materials Science and Engineering: A, 788 (2020).

[6] Y. Qiao, N. Zhao, H. Ma, Heredity of preferred orientation of β-Sn grains in Cu/SAC305/Cu micro solder joints, Journal of Alloys and Compounds, 868 (2021).

[7] H. Shao, A. Wu, Y. Bao, Y. Zhao, G. Zou, L. Liu, Thermal reliability investigation of Ag-Sn TLP bonds for high-temperature power electronics application, Microelectronics Reliability, 91 (2018) 38-45.

[8] H. Shao, A. Wu, Y. Bao, Y. Zhao, G. Zou, Microstructure characterization and mechanical behavior for Ag_3Sn joint produced by foil-based TLP bonding in air atmosphere, Materials Science and Engineering: A, 680 (2017) 221-231.

[9] L. Sun, M.-h. Chen, L. Zhang, P. He, L.-s. Xie, Recent progress in SLID bonding in novel 3D-IC technologies, Journal of Alloys and Compounds, 818 (2020).

[10] K. Chu, Y. Sohn, C. Moon, A comparative study of Cn/Sn/Cu and Ni/Sn/Ni solder joints for low temperature stable transient liquid phase bonding, Scripta Materialia, 109 (2015) 113-117.

[11] J.F. Li, P.A. Agyakwa, C.M. Johnson, Kinetics of Ag_3Sn growth in Ag–Sn–Ag system during transient liquid phase soldering process, Acta Materialia, 58 (2010) 3429-3443.

[12] Y. Qiao, H. Ma, N. Zhao, Diffusion anisotropy induced uneven regional growth of Cu_6Sn_5 IMC in Cu/SAC305/Cu micro solder joints under temperature gradient, Journal of Alloys and Compounds, 886 (2021).

[13] H.J. Dong, Z.L. Li, X.G. Song, H.Y. Zhao, H. Tian, J.H. Liu, J.C. Yan, Grain morphology evolution and mechanical strength change of intermetallic joints formed in Ni/Sn/Cu system with variety of transient liquid phase soldering temperatures, Materials Science and Engineering: A, 705 (2017) 360-365.

[14] H.-K. Cheng, Y.-J. Lin, C.-M. Chen, K.-C. Liu, Y.-L. Wang, T.-F. Liu, Microstructural Evolution of Cu/Solder/Cu Pillar-Type Structures with Different Diffusion Barriers, Metallurgical and Materials Transactions A, 47 (2016) 3971-3980.

[15] J.F. Li, P.A. Agyakwa, C.M. Johnson, Interfacial reaction in Cu/Sn/Cu system during the transient liquid phase soldering process, Acta Materialia, 59 (2011) 1198-1211.

[16] H. Shao, A. Wu, Y. Bao, Y. Zhao, G. Zou, L. Liu, Novel transient liquid phase bonding through capillary action for high-temperature power devices packaging, Materials Science and Engineering: A, 724 (2018) 231-238.

[17] Z. Cai, A. Li, W. Zhang, Y. Zhang, L. Cui, J. Liu, Hierarchical Cu@Co-decorated CuO@Co3O4 nanostructure on Cu foam as efficient self-supported catalyst for hydrogen evolution reaction, Journal of Alloys and Compounds, 882 (2021).

[18] L.-z. ZHAO, M.-j. ZHAO, N. LI, H. YAN, J.-s. ZHANG, Microstructure of nickel foam/Mg double interpenetrating composites, Transactions of Nonferrous Metals Society of China, 20 (2010).

[19] L.Y. Aguirre-Perales, I.-H. Jung, R.A.L. Drew, Foaming behavior of powder metallurgical Al–Sn foams, Acta Materialia, 60 (2012) 759-769.

[20] N. Michailidis, F. Stergioudi, A. Tsouknidas, Deformation and energy absorption properties of powder-metallurgy produced Al foams, Materials Science and Engineering: A, 528 (2011) 7222-7227.

[21] H. Zhang, F. Sun, Y. Liu, Copper foam enhanced Sn58Bi solder joint with high performance for low temperature packaging, Materials Letters, 241 (2019) 108-110.

[22] H. He, S. Huang, Y. Xiao, R. Goodall, Diffusion reaction-induced microstructure and strength evolution of Cu joints bonded with Sn-based solder containing Ni-foam, Materials Letters, 281 (2020).

[23] H. He, S. Huang, Y. Ye, Y. Xiao, Z. Zhang, M. Li, R. Goodall, Microstructure and mechanical properties of Cu joints soldered with a Sn-based composite solder, reinforced by metal foam, Journal of Alloys and Compounds, 845 (2020).

[24] Y. Xiao, Q. Wang, L. Wang, X. Zeng, M. Li, Z. Wang, X. Zhang, X. Zhu, Ultrasonic soldering of Cu alloy using Ni-foam/Sn composite interlayer, Ultrason Sonochem, 45 (2018) 223-230.

[25] L.J. Huang, L. Geng, H.-X. Peng, Microstructurally inhomogeneous composites: Is a homogeneous reinforcement distribution optimal?, Progress in Materials Science, 71 (2015).

[26] H. Han, Y.C. Sohn, J. Yu, Interfacial Reactions between Cu_xNi_y Alloy Underbump Metallurgy and Sn-Ag-zCu Solders, Journal of Electronic Materials, 36 (2007) 578-586.

[27] S.-w. Chen, C.-h. Wang, Interfacial reactions of Sn-Cu/Ni couples at 250 °C, Journal of Materials Research, 21 (2011) 2270-2277.

[28] C. Wang, S. Chen, Sn–0.7wt.%Cu/Ni interfacial reactions at 250°C, Acta Materialia, 54 (2006) 247-253.

[29] C.E. Ho, M.K. Lu, P.T. Lee, Y.H. Huang, W.L. Chou, TEM investigation of interfacial microstructure and fracture mode of the Sn-Ag-Cu/Ni joint system, Materials Science and Engineering: A, 706 (2017) 269-278.

[30] S.J. Wang, C.Y. Liu, Study of interaction between Cu-Sn and Ni-Sn interfacial reactions by Ni-Sn3.5Ag-Cu sandwich structure, Journal of Electronic Materials, 32 (2003).

[31] C.-h. Wang, W.-h. Lai, S.-w. Chen, Dissolution and Interfacial Reactions of $(Cu,Ni)_6Sn_5$ Intermetallic Compound in Molten Sn-Cu-Ni Solders, Journal of Electronic Materials, 43 (2013) 195-203.

[32] C.W. Chang, S.C. Yang, C.-T. Tu, C.R. Kao, Cross-Interaction between Ni and Cu across Sn Layers with Different Thickness, Journal of Electronic Materials, 36 (2007) 1455-1461.

[33] C.E. Ho, R.Y. Tsai, Y.L. Lin, C.R. Kao, Effect of Cu concentration on the reactions between

Sn-Ag-Cu solders and Ni, Journal of Electronic Materials, 31 (2002).

[34] V. Vuorinen, H. Yu, T. Laurila, J.K. Kivilahti, Formation of Intermetallic Compounds Between Liquid Sn and Various $CuNi_x$ Metallizations, Journal of Electronic Materials, 37 (2008) 792-805.

[35] W.-K. Liao, C.-M. Chen, M.-T. Lin, C.-H. Wang, Enhanced growth of the Ni_3Sn_4 phase at the Sn/Ni interface subjected to strains, Scripta Materialia, 65 (2011) 691-694.

[36] J. Görlich, D. Baither, G. Schmitz, Reaction kinetics of Ni/Sn soldering reaction, Acta Materialia, 58 (2010) 3187-3197.

[37] J. Yang, J. Huang, D. Fan, S. Chen, X. Zhao, Structural, mechanical, thermo-physical and electronic properties of η'-$(CuNi)_6Sn_5$ intermetallic compounds: First-principle calculations, Journal of Molecular Structure, 1112 (2016) 53-62.

[38] J.-W. Yoon, B.-I. Noh, J.-H. Yoon, H.-B. Kang, S.-B. Jung, Sequential interfacial intermetallic compound formation of Cu_6Sn_5 and Ni_3Sn_4 between Sn–Ag–Cu solder and ENEPIG substrate during a reflow process, Journal of Alloys and Compounds, 509 (2011) L153-L156.

[39] S. Ren, M. Sun, Z. Jin, Y. Guo, H. Ling, A.-m. Hu, M. Li, Formation Mechanism of Novel Sidewall Intermetallic Compounds in Micron Level Sn/Ni/Cu Bumps, Electronic Materials Letters, 15 (2019) 562-571.

[40] G. Ghosh, Elastic properties, hardness, and indentation fracture toughness of intermetallics relevant to electronic packaging, Journal of Materials Research, 19 (2004) 1439-1454.

[41] J.W. Xian, G. Zeng, S.A. Belyakov, Q. Gu, K. Nogita, C.M. Gourlay, Anisotropic thermal expansion of Ni_3Sn_4, Ag_3Sn, Cu_3Sn, Cu_6Sn_5 and βSn, Intermetallics, 91 (2017) 50-64.

Table 1 EDS results for the analyzed points shown in **Fig. 3**.

Positions	Element composition (at.%)				Phase constitutions
	Ni	Cu	Ag	Sn	
A1	22.18	31.96		45.86	$(Cu,Ni)_6Sn_5$
A2	36.21	9.41		54.38	$(Ni,Cu)_3Sn_4$

Table. 2 EDS results for the analyzed points shown in **Fig. 5**.

Positions	Element composition (at.%)				Phase constitutions
	Ni	Cu	Ag	Sn	
B1	26.51	27.67		45.82	$(Cu,Ni)_6Sn_5$
B2	36.80	6.58		56.62	$(Ni,Cu)_3Sn_4$
B3	37.35	4.92		57.83	$(Ni,Cu)_3Sn_4$
B4	33.48	11.73		54.79	$(Ni,Cu)_3Sn_4$
B5	22.61	29.79		47.60	$(Cu,Ni)_6Sn_5$
B6	25.40	28.44		46.16	$(Cu,Ni)_6Sn_5$

Table 3 The area fraction of different phases in Ni-Cu/SAC joints soldered for various time

Sample		Area fraction (%)		
		$(Cu,Ni)_6Sn_5$	$(Ni,Cu)_3Sn_4$	Ni-Cu alloy
	5min	15.8	1.9	17.2
Ni18Cu/SAC	10min		18.3	15.7
	15min		17.4	12.5
	5min		20.2	13.7
Ni38Cu/SAC	10min	20.0		15.0
	15min	20.7	1.4	17.3
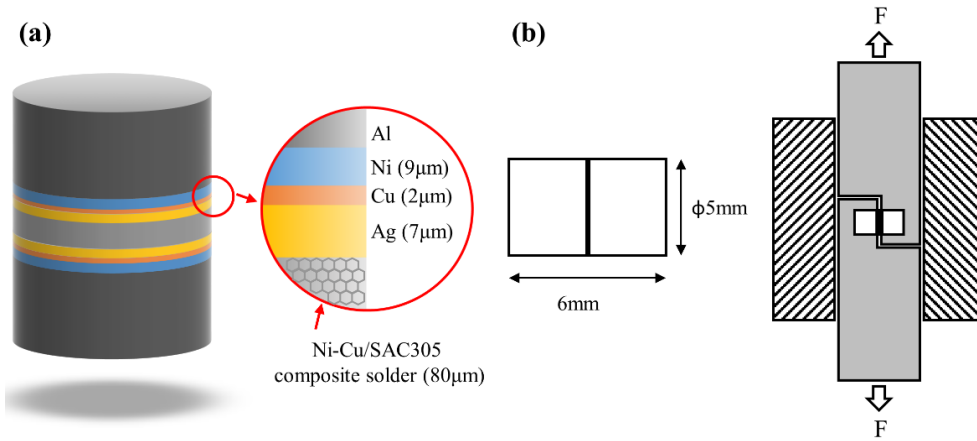
Fig. 1. Schematic diagram for (a) the assembled soldering joint and (b) the shearing

test sample and fixture.
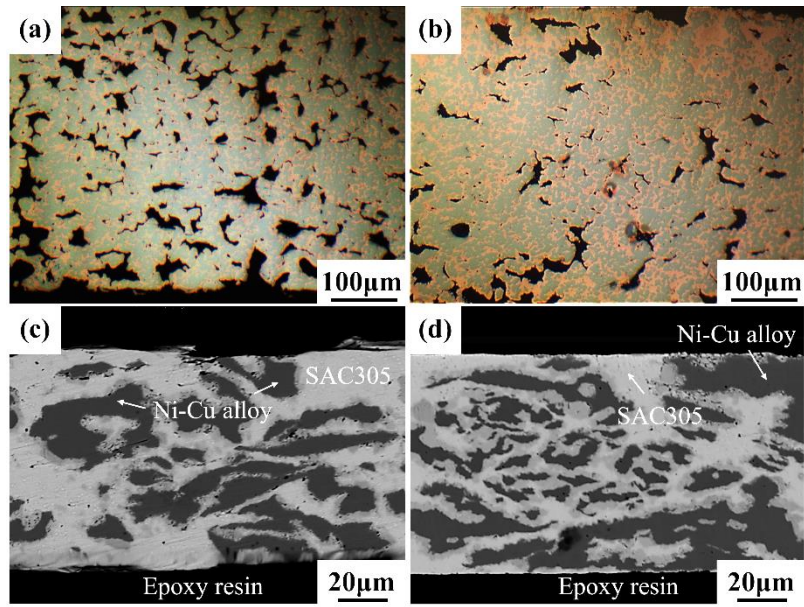
Fig. 2. The cross-section images of (a) Ni18Cu skeleton, (b) Ni38Cu skeleton, (c) Ni18Cu/SAC composite solder, and (d) Ni38Cu/SAC composite solders.
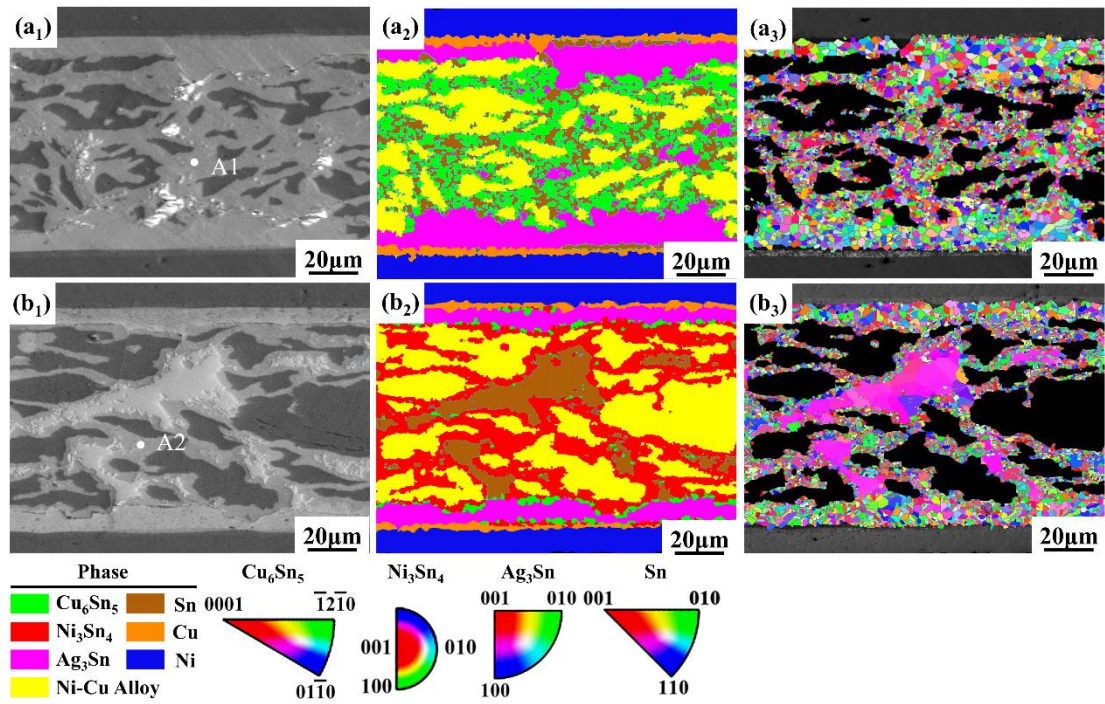
Fig. 3. Cross-section images of Al joints soldered for 1 min using (a) Ni18Cu/SAC and (b) Ni38Cu/SAC composite solders, (1) SEM images, (2) phase distribution, (3) EBSD images for grain distribution.
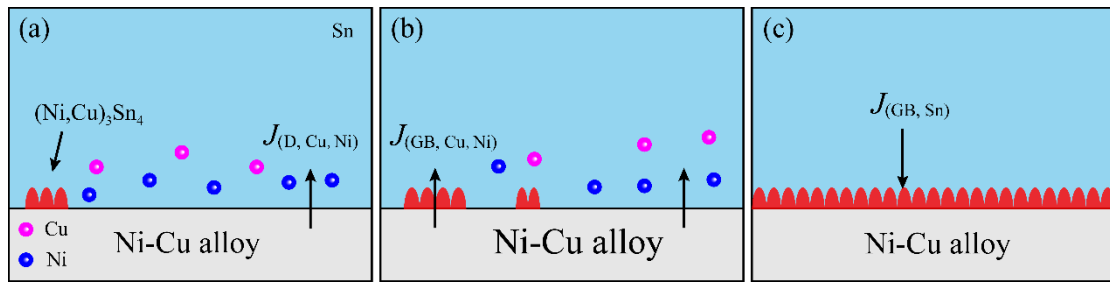
Fig. 4. The schematic diagrams of the (Ni,Cu)$_3$Sn$_4$ formation process for (a) dissolution, (b) dissolution - GB diffusion and (c) GB diffusion.
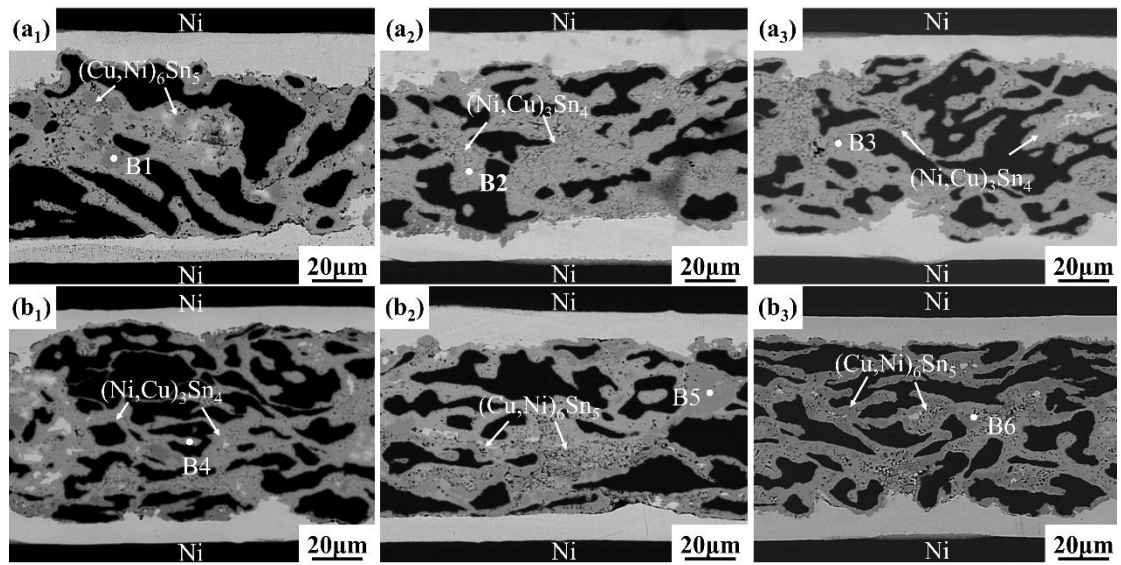
Fig. 5. Cross-section images of Al joints soldered with (a) Ni18Cu/SAC and (b) Ni38Cu/SAC composite solders for (1) 5 min, (2) 10 min, and (3) 15 min.
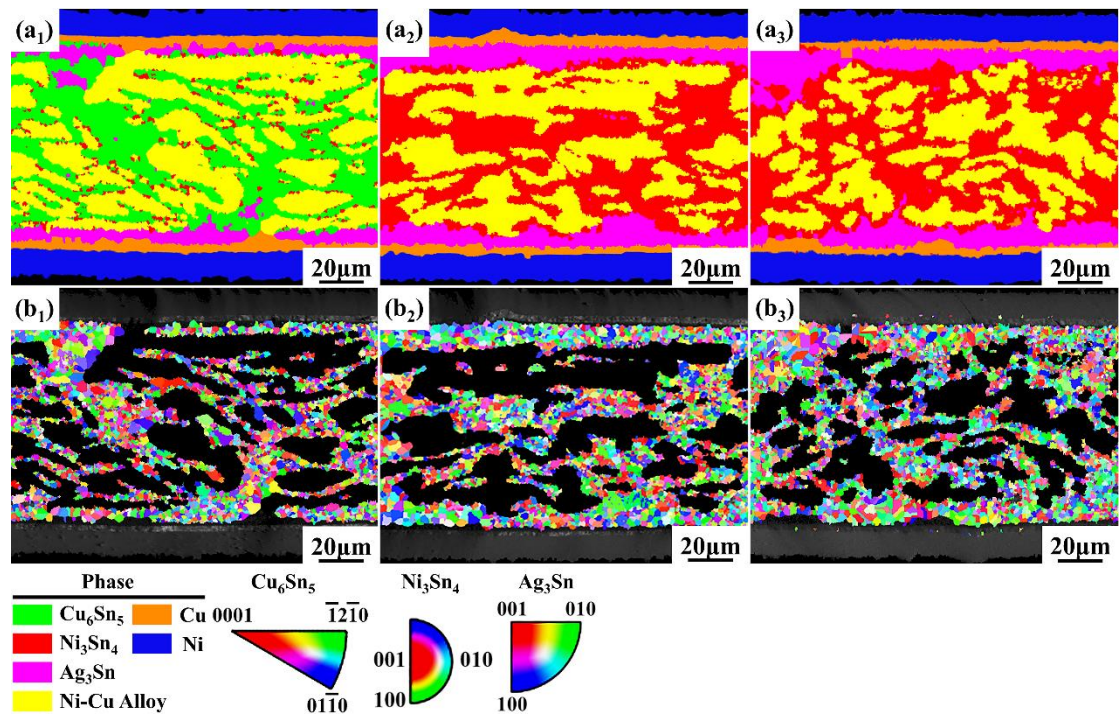
Fig. 6. EBSD images for (a) phase distribution and (b) grain morphology of Al joints soldered with Ni18Cu/SAC composite solder for (1) 5 min, (2) 10 min and (3) 15 min.
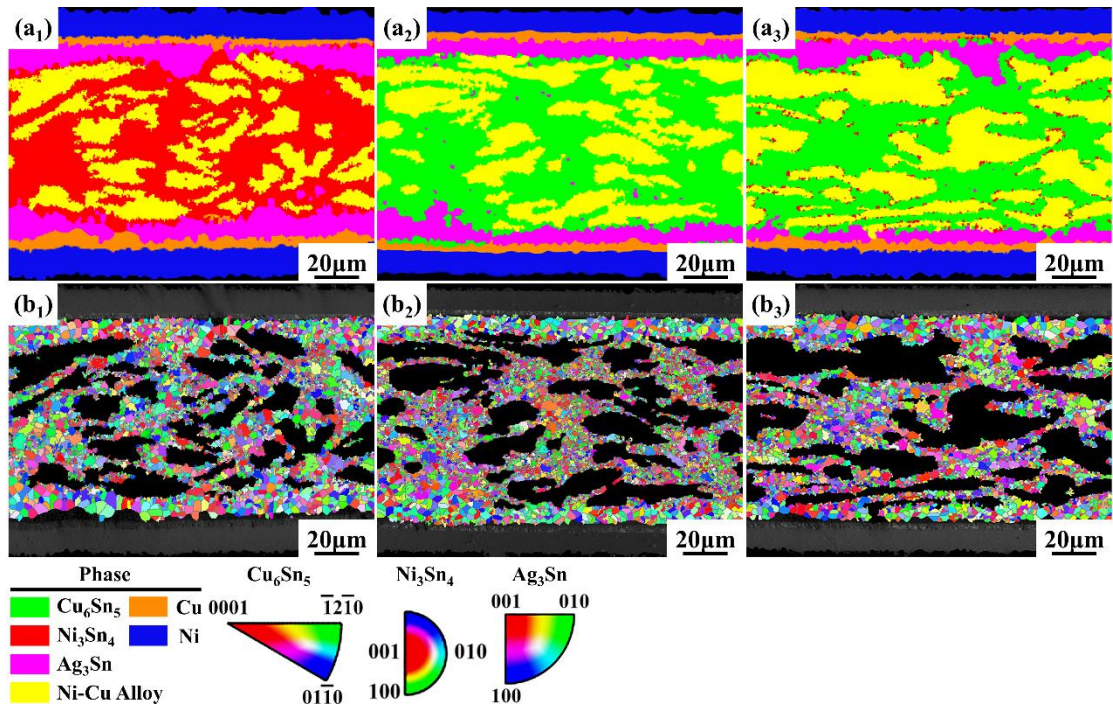
Fig. 7. EBSD images for (a) phase distribution and (b) grain distribution of Al joints soldered with Ni38Cu/SAC composite solder for (1) 5 min, (2) 10 min, and (3) 15 min.
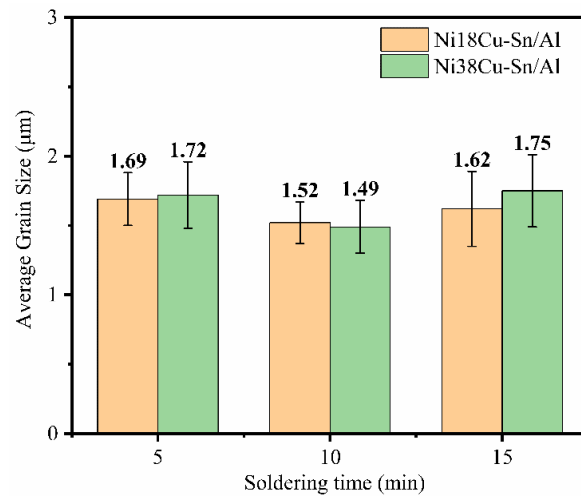
Fig. 8. Average size of $(Cu,Ni)_6Sn_5$ and $(Ni,Cu)_3Sn_4$ grains soldered for various times.
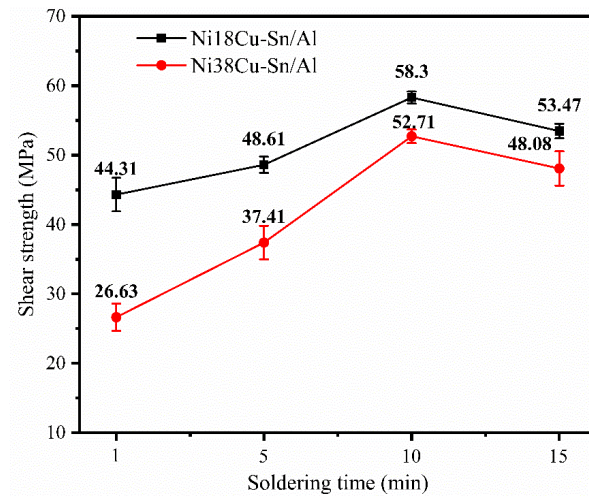
Fig. 9. Shear strength of Al joints soldered with Ni18Cu/SAC and Ni38Cu/SAC composite solders for various times.
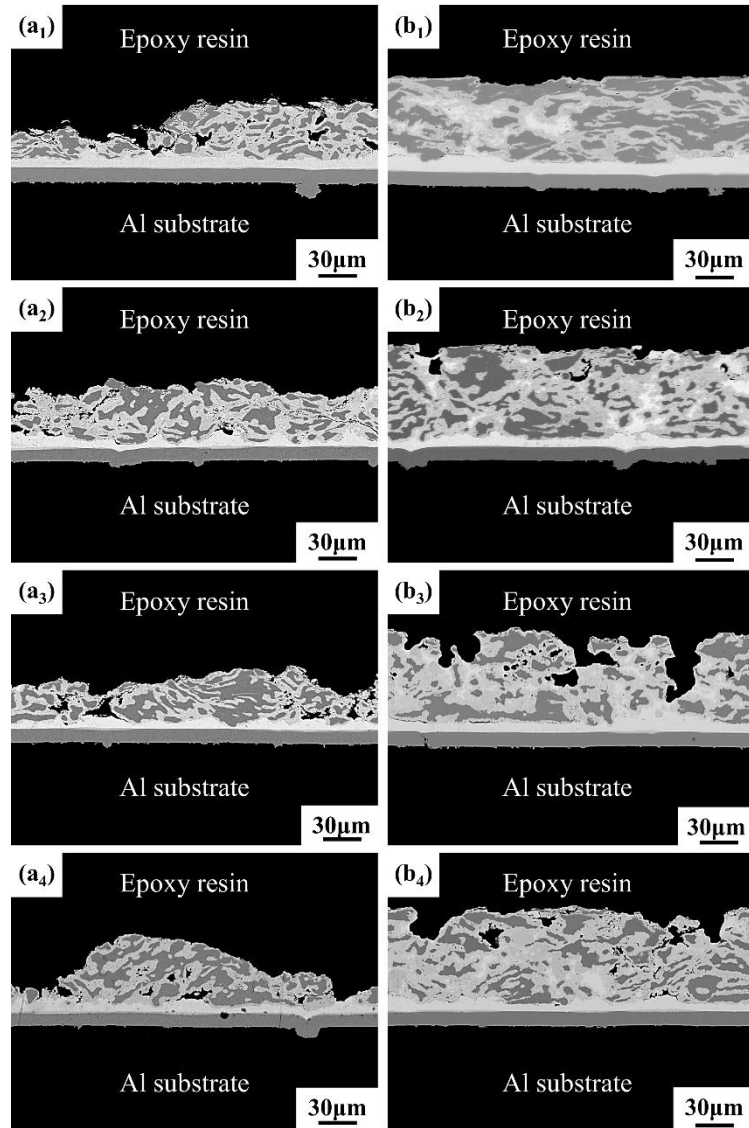
Fig. 10. Cross-section images of fracture joints soldered with (a) Ni18Cu/SAC and (b) Ni38Cu/SAC composite solders for (1) 1 min, (2) 5 min, (3) 10 min, and (4) 15 min.
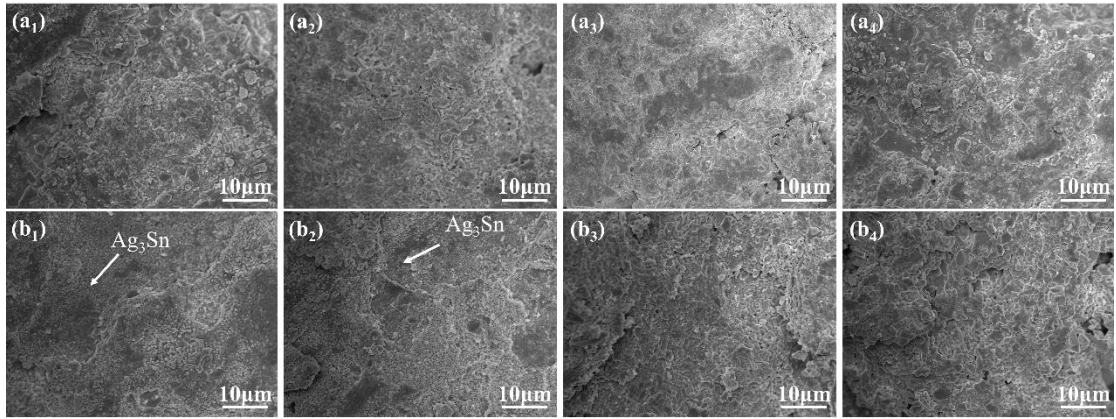
Fig. 11. Top-view SEM images of fracture joints soldered with (a) Ni18Cu/SAC and (b) Ni38Cu/SAC composite solders for (1) 1min, (2) 5min, (3) 10min and (4) 15min.